Journal of Molecular Structure 1225 (2021) 129103

Contents lists available at ScienceDirect

Journal of Molecular Structure

journal homepage: www.elsevier.com/locate/molstr

# Synthesis, in vitro and in silico studies of naphto-1,3-oxazin-3(2*H*)-one derivatives as promising inhibitors of cholinesterase and $\alpha$-glucosidase

Khawla Boudebbous[a], Houssem Boulebd[a,*], Chamseddine Derabli[a,b], Lamia Bendjeddou[c], Chawki Bensouici[d], Dominique Harakat[e], Hocine Merazig[c], Abdelmadjid Debache[a,*]

[a] Laboratory of Synthesis of Molecules with Biological Interest, Frères Mentouri Constantine 1 University, 25000 Constantine, Algeria
[b] National Higher School of Biotechnology "Toufik Khaznadar", Ali Mendjeli University City, 25100 Constantine, Algeria
[c] Research Unit of Environmental Chemistry and Structural Molecular Chemistry, CHEMS, Faculty of Exact Sciences, Tidjani Hadem Campus, Frères Mentouri Constantine 1 University, 25000 Constantine, Algeria
[d] National Research Centre for Biotechnology, 25000 Constantine, Algeria
[e] Reims Champagne-Ardenne University and CNRS, Reims Institute of Molecular Chemistry, UMR 7312, Reims, France

ARTICLE INFO

*Article history:*
Received 27 July 2020
Revised 16 August 2020
Accepted 18 August 2020
Available online 18 August 2020

*Keywords:*
Naphthoxazinone
Phenylboronic acid
Cholinesterase
$\alpha$-Glucosidase
DFT calculations

ABSTRACT

Various substituted naphto-1,3-oxazin-3(2H)-one derivatives have been prepared by a three-component one-pot condensation reaction of 2-naphthol, aromatic aldehydes, and urea using phenylboronic acid as catalyst. The molecular structures of the synthesized compounds were characterized by physical and spectroscopic techniques and, for compound **4b**, by single crystal X-ray diffraction analysis. The cholinesterase and $\alpha$-glucosidase inhibitory activities of the titled compounds have been investigated *in vitro*. The obtained results revealed that some of the synthesized compounds are highly active towards both AChE/BChE and $\alpha$-Glucosidase with $IC_{50}$ values lower than those of the standards galanthamine and acarbose. *In Silico* studies such as Hirshfeld surface, docking study, DFT calculations, and ADME properties have been also performed in order to get insights into the molecular structure, chemical reactivity, structure-activity relationship, and bioavailability of the synthesized compounds.



## 1. Introduction

Alzheimer's disease (AD) is chronic neurodegenerative illness with a complex pathogenesis [1,2]. Due to complexity of the disease, only symptomatic treatment is available up to present. AD is frequently affiliated with damage of cholinergic system in the brain, characterized by progressive memory loss, with decline in language and finally even losing control of bodily functions, are due, among other causes, progressive accumulation of $\beta$ amyloid proteins (A$\beta$) together with tau ($\beta$)-protein aggregation leading to shrinkage and death of neurons [3]. The researchers are focused on cholinergic hypothesis because it has become the most leading theory to explain etiology of the disease. Furthermore, almost all hypotheses had devoted that increase the level of acetylcholine in cholinergic synapses in the brain by inhibiting acetylcholinesterase (AChE) could effectively improve the cognitive functions and memory ability [4]. Nowadays, cholinesterase (ChE) became one of major targets in the current therapy of AD [5], and most of the drugs approved by the Food and Drug Administration (FDA) for the AD therapy are AChE inhibitors including tacrine, rivastigmine, donepezil, and galantamine but they have severe adverse effects such as hepatotoxicity and anxiety [6,7].

Diabetes mellitus (DM) is another chronic metabolic disorder, characterized by excessive levels of glucose in the blood [7], resulted from defects in the action or secretion of insulin. $\alpha$-Glucosidase, a membrane bound enzyme present in the epithelial wall of the small intestine, is responsible for digestion of carbohydrate and release of glucose. In human, this metabolic disorder results in serious health complication associated with various diseases including cardiovascular, neuropathy problems, retinopathy, amputations, impaired wound healing and cancer [8]. $\alpha$-Glucosidase enzyme is the restorative target to treat diabetes [9] and its inhibitors play an important role for treatment of DM by decreasing sugar level in the bloodstream [10,11]. Currently, $\alpha$-glucosidase inhibitors such as acarbose, voglibose, and miglitol are approved for the treatment of type-2 diabetes, but they are associated with common undesirable effects including gastrointestinal diseases flatulence, and diarrhea [12,13].

On the other hand, naphthoxazine derivatives and their analogues exhibit a variety of interesting biological properties such

* Corresponding authors.
*E-mail addresses:* boulebd.houssem@umc.edu.dz (H. Boulebd), a_debache@yahoo.fr (A. Debache).

https://doi.org/10.1016/j.molstruc.2020.129103
0022-2860/

as 5-HT ligands [14], platelet fibrinogen receptor antagonists [15], protein kinase [16], HIV inhibitor [17], anti-viral [18], antimicrobial [19], antitumor [20], antimalarial [21], hypertensive [22], and antiarrhythmic [23]. In addition, molecules with 1,3-amino oxygen functions have been reported to have a variety of biological and pharmacological activities, including nucleoside antibiotics [24] and HIV protease inhibitors [25], and are frequently found in biologically active natural products [26]. The search for new procedures for the synthesis of naphthoxazine derivatives remains a constant preoccupation of organic chemists with the aim of improving yields, reaction times and, as far as possible, respecting the environment. Currently the best synthesis method for naphthoxazinone derivatives is the multicomponent reaction between 2-naphthol, aromatic aldehydes and urea in the presence of a variety of catalysts such as *p*-TSA [27], [bmim]Br [28], tetramethylammonium hydroxide [29], silica-bonded S-sulfonic acid [30], Thiamine hydrochloride [31], $TiCl_4$ [32], Cu [33], and ZnO [34].

In continuation of our work focused on the development of novel heterocyclic compounds that may be useful in the treatment of chronic disorders such as Alzheimer's disease or diabetes mellitus, we are focusing on naphthoxazinone derivatives [35–38]. In this study, we aimed to investigate the *in vitro* AChE, BChE, and $\alpha$-glucosidase inhibitory activities of a series of naphthoxazinone derivatives to determine their potential for the treatments of AD and DM. Furthermore, *In Silico* studies such as Hirshfeld surface, docking study, DFT calculations, and ADME properties were performed in order to support the experimental results.

## 2. Experimental section

### 2.1. Materials and equipments

The reagents and solvents are used without any further purification. The melting points were determined using a digital Electrothermal IA9100 apparatus. IR spectra were obtained in the form of potassium bromide pellets (KBr) Shimadzu FT IR-8201 PC spectrometer. $^1$H and $^{13}$C NMR spectra were recorded on a Bruker Advance DPX spectrometer at 250.13 and 62.5 MHz respectively with the TMS as internal reference. Mass spectrometry experiments were performed in positive mode, on a Synapt-G2 HDMS Traveling Wave-Ion Mobility (TWIMS) instrument equipped with an electrospray ionization source (Waters, Manchester, UK). Kieselgel $F_{254}$ (Merck) plates have been used in TLC. Crystal suitable for single crystal X-ray diffraction was selected using a polarizing microscope. The crystal was coated with Paratone oil and mounted on a loop for data collection and the lattice parameters were determined using a Bruker APEX II CCD diffractometer (SADABS; Sheldrick, 2002). All activities were established with a thermo Electron Corporation spectrophotometer type Helios Delta. The measurements were carried out on a 96-well microplate reader, PerkinElmer Multimode Plate Reader EnSpire, USA.

### 2.2. Synthesis

#### 2.2.1. Synthesis of 1,2-Dihydro-1-arylnaphtho[1,2-e][1,3]oxazine-3-one (4a-f)

Phenylboronic acid (0.15 mmol) was added to a mixture of 2-naphthol (2.0 mmol), aldehyde (2.4 mmol), and urea (2.4 mmol). The resulting mixture was magnetically heated at 120 °C without solvent for the appropriate time. After completion (TLC), the reaction mixture was allowed to warm to room temperature, then 5 ml of iced water was added while maintaining stirring for 30 min. The solid product was filtered and purified by column chromatography on silica gel (Ethyl acetate: *n*-Hexane, 1: 2) to afforded the title compounds.

*1-phenyl-1H-naphtho[1,2-e][1,3]oxazin-3(2H)-one* (***4a***). White solid (75%). IR (KBr): $\nu$ ($cm^{-1}$) 3217, 2924, 2848, 2355, 1666, 1624, 1512, 1436, 1265; $^1$H NMR (DMSO-$d_6$, 300 MHz): $\delta$ (ppm) 9.74 (d, *J*= 2.7 Hz, 1H, NH), 7.99 (d, *J*= 9.0 Hz, 1H, Ar), 7.95 (dd, *J*=7.2 Hz, *J*= 1.8 Hz, 1H, Ar), 7.82 (d, *J*= 7.8 Hz, 1H, Ar), 7.51-7.43 (m, 2H, Ar), 7.39 (d, *J*= 8.7 Hz, 1H, Ar), 7.33-7.22 (m, 5H, Ar), 6.20 (d, *J*= 2.7 Hz, 1H, $-CH_{sp3}$); $^{13}$C NMR (DMSO-$d_6$, 75 MHz): $\delta$ (ppm) 149.3, 147.4, 142.9, 130.4, 130.2, 129.0, 128.9, 128.6, 128.0, 127.4, 127.0, 125.1, 123.1, 116.9, 114.1, 53.8.

*1-(3-Bromo-4-methoxy-phenyl)-1,2-dihydro-naphtho[1,2-e][1,3] oxazin-3-one* (***4b***). White crystals (72%). IR (KBr): $\nu$ ($cm^{-1}$) 3221, 3144,2964,1732, 1517, 1439, 1224; $^1$H NMR (DMSO-$d_6$, 250 MHz): $\delta$ (ppm) 8.67 (d, *J*= 2.6 Hz, 1H, –NH), 7.87–7.81 (m, 2H, Ar), 7.58 (d, *J*= 8.4 Hz, 1H, Ar), 7.47–7.34 (m, 3H, Ar), 7.25 (d, *J*= 8.9 Hz, 1H, Ar), 7.1 (dd, *J*= 8.4 Hz, *J*= 1.9 Hz, 1H, Ar), 6.8 (d, *J*= 8.5 Hz, 1H, Ar), 6.0 (d, *J*= 2.6 Hz, 1H, $-CH_{sp3}$), 3.76 (s, 3H, $-OCH_3$); $^{13}$C NMR (DMSO-$d_6$, 62.9 MHz): $\delta$ (ppm) 155.1, 149.4, 147.4, 135.9, 131.5, 130.3, 130.1, 128.8, 128.4, 127.2, 124.8, 122.5, 119.1, 116.6, 112.9, 112.1, 111.1, 55.9, 53.1; HRMS ($ESI^+$): m/z $[M+Na]^+$calculated for $C_{19}H_{14}NO_3NaBr$ 406.0055, found 406.0045.

*1-Biphenyl-4-yl-1,2-dihydro-naphtho[1,2-e][1,3]oxazin-3-one* (***4c***). White-yellow crystals (66%). IR (KBr): $\nu$ ($cm^{-1}$) 3222, 3140, 2924, 1731, 1513, 1437, 1222; $^1$H NMR (DMSO-$d_6$, 250MHz): $\delta$ (ppm) 7.90 (d, *J*= 8.8 Hz, 1H), 7.88 (d, *J*= 8.8 Hz, 1H), 7.65–7.58 (m, 2H), 7.55–7.43 (m, 7H), 7.42–7.29 (m, 4H), 7.10 (s, 1H), 6.20 (s, 1H); $^{13}$C NMR (DMSO-$d_6$, 62.9 MHz): $\delta$ (ppm) 150.8, 147.7, 141.6, 140.7, 140.3, 131.1, 130.7, 129.4, 129.0, 128.9, 128.2, 127.6, 127.6, 127.2, 125.4, 123.0, 117.2, 112.6, 55.7; HRMS ($ESI^+$): m/z $[M+Na]^+$calculated for $C_{24}H_{17}NO_2Na$ 374.1157, found 374.1151.

*1-(thiophen-2-yl)-1, 2-dihydro-3H-naphtho[1,2-e][1,3]oxazin-3-one* (***4d***). Green solid (68%). IR (KBr): $\nu$ ($cm^{-1}$) 3258, 3166, 2925, 1743, 1703, 1515, 1389, 1219, 1175, 725; $^1$H NMR (DMSO-$d_6$, 250 MHz): $\delta$ (ppm) 8.96 (d, *J*= 2.9 Hz, 1H, NH), 7.92-7.84 (m, 3H, Ar),7.52-7.40 (m, 2H, Ar), 7.28 (dd, *J*=5.2 Hz, *J*=1.1 Hz, 1H, Ar), 7.09 (d, *J*= 3.2 Hz, 1H, Ar), 6.90 (dd, *J*= 4.9 Hz, *J*=3.6 Hz, 1H, Ar), 6.46 (d, *J*= 2.9 Hz, 1H, $-CH_{sp3}$); $^{13}$C NMR (DMSO-$d_6$, 62.9MHz): $\delta$ (ppm) 149.5, 147.1, 146.5, 130.2, 130.1, 128.8, 128.4, 127.2, 126.6, 125.7, 125.3, 124.9, 122.6, 116.6, 114.0, 48.9; HRMS ($ESI^+$): m/z $[M+H]^+$calculated for $C_{16}H_{12}NO_2S$ 282.0589, found 282.0587.

*1-(4-ethylphenyl)-1H-naphtho[1,2-e][1,3]oxazin-3(2H)-one* (***4e***). Beige solid (60%). IR (KBr): $\nu$ ($cm^{-1}$) 3216, 3143, 2962, 2925, 1731, 1513, 1386, 1218, 808;$^1$H NMR (DMSO-$d_6$, 250 MHz): $\delta$ (ppm) 8.85 (d, *J*= 2.9 Hz, 1H, NH), 8.00–7.92 (m, 2H), 7.83 (dd, *J*= 8.1 Hz, *J*= 1.3 Hz, 1H, Ar), 7.51–7.36 (m, 3H, Ar), 7.24 (d, *J*= 8.1 Hz, 2H, Ar), 7.15 (d, *J*= 8.1 Hz, 2H, Ar), 6.17 (d, *J*= 2.9 Hz, 1H, $-CH_{sp3}$), 2.51 (q, *J*= 7.5 Hz, 2H, $-CH_2$), 1.10 (t, *J*= 7.5 Hz, 3H, $-CH_3$); $^{13}$C NMR (DMSO-$d_6$, 62.9MHz): $\delta$ (ppm) 149.4, 147.4, 143.6, 140.3, 130.4, 130.1, 128.9, 128.6, 128.3, 127.3, 126.9, 125.1, 123.1, 116.9, 114.2, 53.6, 27.8, 15.5.

*1-(2-bromophenyl)-1H-naphtho[1,2-e][1,3]oxazin-3(2H)-one* (***4f***). Orange-yellow solid (65%). IR (KBr): $\nu$ ($cm^{-1}$) 3251, 3147, 2921, 1723, 1516, 1381, 1221, 742; $^1$H NMR (DMSO-$d_6$, 250 MHz): $\delta$ (ppm) 8.95 (d, *J*= 2.2 Hz, 1H, NH), 8.03 (d, *J*=8.9 Hz, 1H, Ar), 7.97 (d, *J*=7.5 Hz, 1H, Ar), 7.70 (dd, *J*= 7.9 Hz, *J*= 1.2 Hz, 1H, Ar), 7.58-7.39 (m, 4H, Ar), 7.33-7.19 (m, 2H, Ar), 7.13 (dd, *J*= 7.4 Hz, *J*= 1.5 Hz, 1H, Ar), 6.48 (d, *J*= 2.5 Hz, 1H, $-CH_{sp3}$);$^{13}$C NMR (DMSO-$d_6$, 62.9MHz): $\delta$ (ppm) 148.6, 147.8, 141.2, 133.3, 130.7, 130.5, 130.3, 129.7, 129.1, 128.9, 128.8, 127.7, 125.2, 122.4, 122.2, 116.9, 112.9, 54.1; HRMS ($ESI^+$): m/z $[M+H]^+$calculated for $C_{18}H_{13}NO_2Br$ 354.0130, found 354.0128.

### 2.3. Crystal structure analysis

X-ray diffraction data were acquired at 293 K on a Bruker APEX II CCD diffractometer employing graphite crystal monochromatized MoK$\alpha$ radiation source (0.71073A). Data collection,

**Table 1**
Single-crystal X-ray data and structure refinement details for **4b**.

| Compound | 4b |
|---|---|
| Formula | $C_{19}H_{14}BrNO_3$ |
| M r | 384.21 |
| Temperature/K | 293 |
| Wavelength/Å | 0.71073 |
| Crystal system | Monoclinic |
| Space group, N | $P2_1/c$, 14 |
| a/Å | 11.4377(5) |
| b/Å | 17.1812(7) |
| c/Å | 9.1941(4) |
| $\alpha$/ ° | 90 |
| $\beta$/ ° | 112.806(2) |
| $\gamma$ / ° | 90 |
| V/Å$^3$ | 1665.52(12) |
| Z | 4 |
| $D_c$ (g cm Å$^{-3}$) | 1.532 |
| $\mu$ | 2.48 |
| No. of measured, independent and observed [$I \geq 2\sigma(I)$] reflections | 19920/5066/2781 |
| Absorption correction | Multi-scan |
| $T_{min}$, $T_{max}$ | 0.633, 0.746 |
| $R_{int}$ | 0.040 |
| Data/restraints/parameters | 5066/0/217 |
| $R_1$ /w$R_2$ [I > 2$\sigma$(I)] | 0.046/0.126 |
| Goodness-of-fit on F$^2$ | 1.01 |
| $\Delta\rho_{max}$, $\Delta\rho_{min}$ (e Å$^{-3}$) | 0.79/-070 |

indexing with reduction and absorption corrections were carried out using APEX2, SAINT and SADABS programs, respectively. The structure was solved using direct methods (SIR92) [39] and refined by full-matrix least-squares techniques on F2 with SHELXL-2014 [40] operating within WinGX [41]. All non-H atoms were refined anisotropically. All H atoms were positioned geometrically and refined as riding atoms, with N–H = 0.86, C–H = 0.93, 0.96 and 0.98 aromatic, methylene, acetylenic and methane respectively, and constrained to ride on their parent atoms, with U iso (H) = 1.2U eq (C, N). General crystallographic details for compound **4b** are provided in Table 1. The final atomic coordinates, selected bond distances, and bond angles are presented in Tables S1–S3 (supporting information), respectively. The crystal of compound **4b** belong to monoclinic systems with a centrosymmetric space group of $P2_1/c$. The figures were made using the Mercury and POV-Ray programs [42]. Complete crystallographic data for the structural analysis have been deposited with the Cambridge Crystallographic Data Centre; CCDC reference number 1982885. These data can be obtained free of charge via www.ccdc.cam.ac.uk/conts/retrieving.html (or from the Cambridge Crystallographic Data Centre, 12 Union Road, Cambridge CB2 1EZ, UK; fax: (+44) 1223 336033; e-mail: deposit@ccdc.cam.uk).

### 2.4. Computational details

Molecular structure of compound 4b (representative molecule) was optimized using DFT calculations starting from the crystal structure coordinates. The Becke's three parameters Lee-Yang-Parr exchange correlation functional (B3LYP) [43,44] and the 6-311++G(d,p) basis set have been used for all calculations [45]. The accuracy of this methodology has been confirmed by previous studies [46]. Vibrational frequency analysis was employed to confirm the ground state (no imaginary frequency). Electronegativity, chemical softness, chemical hardness, and electrophilic index were calculated from the frontier molecular orbitals energies method as reported in our previous studies [47–50]. All calculations have been performed using Gaussian09 software [51]. Crystal Explorer 17.5 software has been used to generate the Hirshfeld surface [52]. ADME properties were calculated by using Molinspiration online property calculation toolkit (available at: http://www.molinspiration.com).

### 2.5. Anticholinesterase activity assay

Acetylcholinesterase (AChE) and butyrylcholinesterase (BChE) inhibitory activity was measured, by the spectrophotometric method developed by Ellman et al [53]. Briefly, 150 µL of 100 mM sodium phosphate buffer (pH 8.0), 10 µL of sample solution dissolved in methanol at different concentrations and 20 µL AChE ($5.32 \times 10^{-3}$ U) or BChE ($6.85 \times 10^{-3}$U) solution were mixed and incubated for 15 min at 25°C, and 10 µl of 0.5 mM DTNB [5,5ᐟdithio-bis(2-nitrobenzoic) acid] were added. The reaction was then initiated by the addition of 10 µL of acetylthiocholine iodide (0.71 mM) or butyrylthiocholine chloride (0.2 mM). The hydrolysis of these substrates were monitored spectrophotometrically by the formation of yellow 5-thio-2-nitrobenzoate anion, as the result of the reaction of DTNB with thiocholine, released by the enzymatic hydrolysis of acetylthiocholine iodide or butyrylthiocholine chloride, respectively, at a wavelength of 412 nm, every 5 min for 15 min, utilizing a 96-well microplate reader (Perkin Elmer Multimode Plate Reader EnSpire, USA) in triplicate experiments. Galantamine was used as reference compound. The results were given as 50% inhibition concentration ($IC_{50}$) and the percentage of inhibition of AChE or BChE was determined by comparison of reaction rates of samples relative to blank sample (methanol in phosphate buffer, pH 8) using the equation below:

$$\text{Inhibition of AchE or BChE}(\%) = \frac{E-S}{E} \text{ x } 100$$

Where E is the activity of enzyme without test sample, and S is the activity of enzyme with test sample.

### 2.6. Determination of the α-glucosidase activity

The α-glucosidase capacity of compound was determined using the method described by S. Lordan *et al* [54] with minor modification. Briefly, 50 µL of sample solution at varying concentration and 100 µL of α-glucosidase from *Saccharomyces cerevisiae* (0.1 U/ml) prepared in phosphate buffer were mixed in a 96-wellmicroplate. After 50 µL of *p*-nitrophenyl-α-D-glucopyranoside (PNPG) (5 mM) was then added to each well. The mixture was incubated for 30 min at 37°C and absorbance was read at 405 nm using a microplate reader. The results were compared with those of acarbose and quercetin. The activity was expressed as percentage inhibition using the following equation:

$$\%\,\text{Inhibition} = \left[\frac{A_{control} - A_{sample}}{A_{control}}\right] \times 100$$

Where $A_{control}$ and $A_{sample}$ are the absorbances of the reference and sample obtained from the UV visible spectrophotometer.

### 2.7. Statistical analyses

All the experimental results are mentioned as a mean ± standard deviation of three trials. Significant differences between means were determined by Student's-*t* test, $p<0.05$ were regarded as significant. $IC_{50}$ values, calculated from the concentration-effect linear regression.

### 2.8. Docking study methods

Docking studies of the *R* and *S* enantiomers of the most active compounds (**4b** and **4c**) to the proteins AChE, BChE, and α-glucosidase were carried out with "Achilles" Blind Docking Server

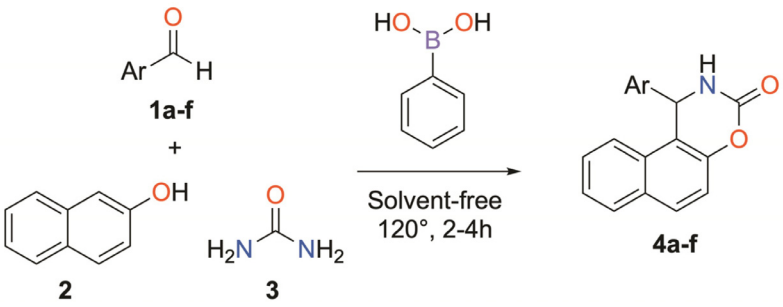


**Scheme 1.** Synthesis of naphthoxazinone **4a-4f** catalyzed by phenylboronic acid.

**Table 2**
Solvent-free synthesis of $\beta$-naphthalene condensed oxazinone derivatives in the presence of phenylboronic acid.

| Compound | Ar | Time (h) | Yield (%)* | Melting point (°C) | |
|---|---|---|---|---|---|
| | | | | Measured | Reported |
| 4a | $C_6H_5$ | 3 | 75 | 218-220 | 217-218 [59] |
| 4b | 3-Br-4-OMe-$C_6H_3$ | 2 | 72 | 216-218 | New |
| 4c | 4-phenyl-$C_6H_4$ | 4 | 66 | 232-233 | 203-206 [59] |
| 4d | 2-thiophenaldehyde | 3 | 68 | 208-209 | 208-210 [60] |
| 4e | 4-Ethyl-$C_6H_4$ | 4 | 60 | 215-217 | 210-213 [61] |
| 4f | 2-Br-$C_6H_4$ | 4 | 65 | 243-245 | New |

* Isolated pure product

(http://bio-hpc.eu/). Using a "blind docking" approach, the docking of the small molecule to the targets is done without a priori knowledge of the location of the binding site by the system [55]. Figures were drawn using the BIOVIA Discovery Studio (https://3dsbiovia.com/). The ligand structures have been built and energy minimized using Gaussian09 program (B3LYP/6-311++G(d,p)). The coordinates of hAChE (PDB ID: 4EY6) [56], hBChE (PDB ID: 4BDS) [57], and $\alpha$-glucosidase (PDB: 5ZCB) [58], were obtained from the Protein Data Bank (PDB) (https://www.rcsb.org).

## 3. Results and discussion

### 3.1. Chemistry

The naphthoxazinone derivatives **4a-f** were synthesized *via* the multicomponent cyclocondensation reaction between aromatic aldehydes (**1a-f**), 2-naphthol (**2**), and urea (**3**) in the presence of phenylboronic acid under solvent-free conditions (Scheme 1). Water was added to the reaction mixture and simply filtering, provides the crude product, which was purified by column chromatography on silica gel (Ethyl acetate: n-Hexane, 1:2) to afford the pure compounds. As results of our experiments we found that aromatic aldehydes containing both electron-withdrawing groups (including halide groups) or electron-donating groups (such as ethyl or alkoxyl groups) reacted well to give the corresponding naphthoxazinone derivatives in good yields. The results are summarized in Table 2. The molecular structures of the synthesized compounds were characterized by physical and spectroscopic techniques (see Experimental section) and, for compound **4b,** by single crystal X-ray diffraction analysis.

### 3.2. Structural description of compound 4b

Single-crystal structure analysis shows that compound **4b** crystallizes in the monoclinic space group $P2_1/c$, with one symmetry-independent molecule in the asymmetric unit (Fig. 1). All bond lengths and angles in **4b** have regular values [62] and comparable with those previously reported [63]. The naphthalene rings systems are essentially planar with maximum deviations from the mean plane of 0.0106 °. The dihedral angle between the fused rings is 3.67 (8)°. The mean plane of the naphthalene ring system subtends a dihedral angle of 82.14 (8)° with the bromo methoxy phenyl ring, while the dihedral angles between the naphthalene ring system and the six-membered ring O(2)/C(16)/N(1)/C(19)/C(14)/C(15) is slightly puckered [64] (6.40 (12) Å). In the solid state, the molecular units of **4b** are interconnected by intermolecular N1–H1···O3$^{i}$ and C12–H12...Br1$^{ii}$ hydrogen bonds [symmetry code: (i)-x+1, -y+1, -z+2, (ii) –x, -y+1, -z+1] (Table 3) which may result in the formation of the dimeric chains running extended to [101] direction with $R^2_2(8)$ and $R^2_2$ (18) motifs [65]. These chains are linked to each other by two hydrogen bonds C–H···$\pi$ type [H10···Cg2$^{iii}$ = 2.78 Å, and C10–H10···Cg2$^{iii}$ = 164° with Cg2 is the centroid of the C1–C6 phenyl ring; H19...Cg4$^{iv}$ = 2.92 Å, and C19-H19···Cg4$^{iv}$ = 143° with Cg4 is the centroid of the C8-C13C14C15C16C17 naphthalene ring, symmetry code: (iii) x, y, z-1, (iv) –x+1, -y, -z] thus generating a three-dimensional network (Fig. 2).

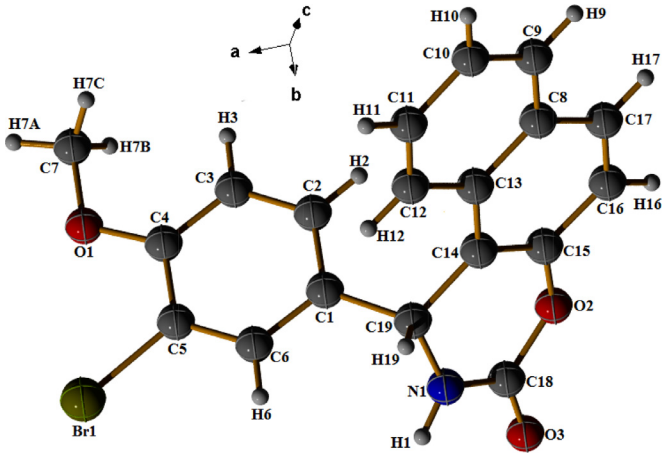


**Fig. 1.** The asymmetric unit of compound **4b**, showing the atom-numbering scheme. Displacement ellipsoids are drawn at the 50% probability level.

**Table 3**
Hydrogen-bond geometry (Å, °) of compound **4b**.

| D-H...A | D-H | H...A | D...A | D-H...A |
|---|---|---|---|---|
| N1-H1...O3$^{i}$ | 0.8600 | 2.0400 | 2.8823(1) | 167.00 |
| C12-H12...Br1$^{ii}$ | 0.9300 | 2. 8500 | 3.6568(2) | 146.00 |
| C10-H10...Cg2$^{iii}$ | 0.9300 | 2.7800 | 3.6832(2) | 164.00 |
| C19-H19...Cg4$^{iv}$ | 0.9300 | 2.9200 | 3.7501(2) | 143.00 |

Symmetry codes : (i) -x+1, -y+1, -z+2; (ii) -x,- y+1, -z+1; (iii) x, y, z-1; (iv) -x+1, -y, -z

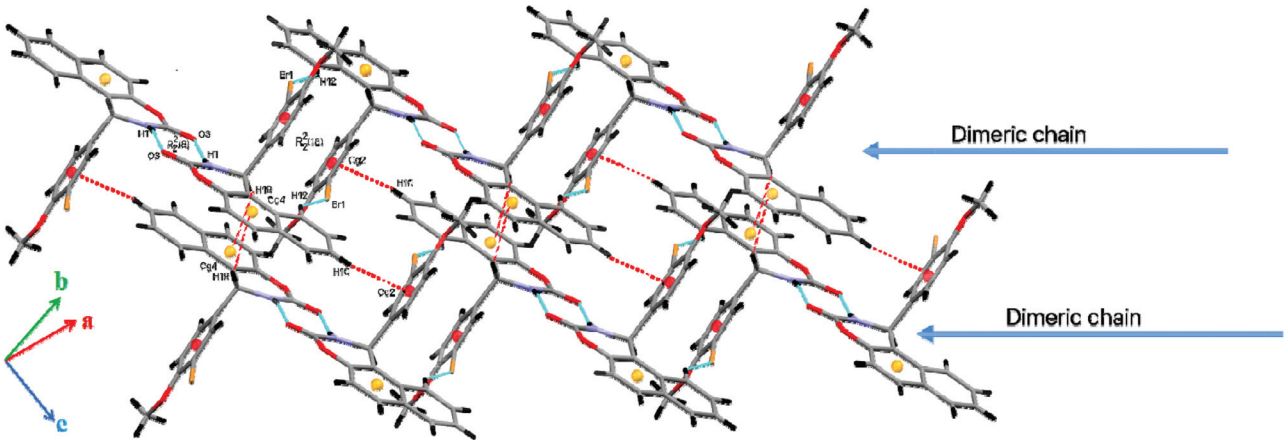


**Fig. 2.** A view of the three-dimensional network of compound **4b**, showing hydrogen bonds.

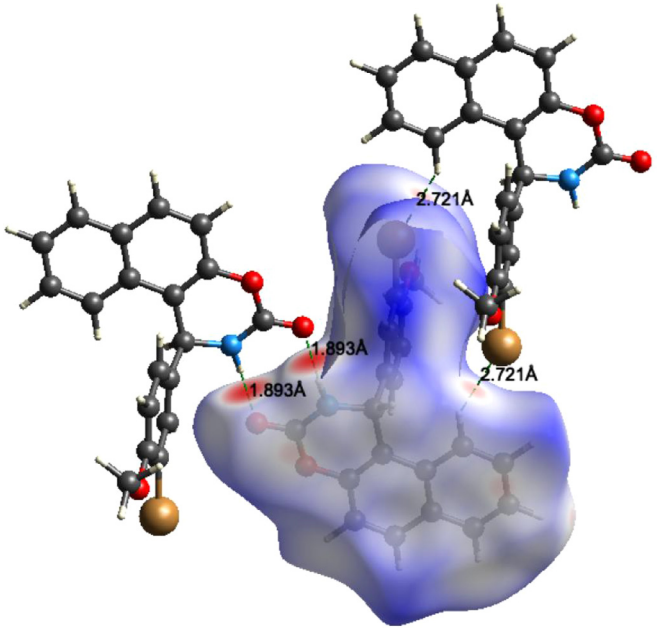


**Fig. 3.** The 3D Hirshfeld surface of compound **4b** mapped over $d_{norm}$ in the range –0.5534 to 1.6107 a. u.

### 3.3. Hirshfeld surface analysis

The Hirshfeld surface of compound **4b** mapped over $d_{norm}$ have been studied in order to quantify the intermolecular contacts of the crystal structure using Crystal Explorer 17.5 software [52]. The three-dimensional Hirshfeld surface and its related two-dimensional fingerprints are presented in Figs. 3 and 4, respectively. As shown from the Hirshfeld surface, compound **4b** forms mainly two strong intermolecular hydrogen bonds between the NH bond (N1–H1) and the carbonyl group (C18–O3) with distances shorter than Van der waals (Vdw) radii (represented by red spots). It forms also several weak intermolecular bonds type CH…O, CH…Br, CH…C with distances nearly equal to the sum of Vdw radii (represented by white areas). The contribution of the different types of contacts are presented as 2D fingerprint plots in Fig 4. As can be seen, the different types of contacts have nearly comparable contributions. The highest contribution was observed for the H…C/C…H (28.0%) contacts followed by H…H/H…H (26.0%), and finally H…O/O…H (23.7%).

**Table 4**
Selected calculated and experimental bond lengths (Å) and angles (°) for compound **4b**.

| | Experimental | Calculated |
|---|---|---|
| Bond lengths (Å) | | |
| Br1-C5 | 1.890(2) | 1.910 |
| O2-C18 | 1.361(3) | 1.376 |
| O2-C15 | 1.392(3) | 1.382 |
| O3-C18 | 1.218(3) | 1.203 |
| C1-C19 | 1.527(3) | 1.529 |
| C19-N1 | 1.459(4) | 1.473 |
| C14-C15 | 1.358(3) | 1.373 |
| Angles (°) | | |
| C18-N1-C19 | 127.9(2) | 125.7 |
| C18-O2-C15 | 119.6(2) | 121.1 |
| O2-C15-C16 | 114.3(2) | 114.8 |
| N1-C18-O2 | 117.9(2) | 115.3 |
| N1-C19-C1 | 110.0(2) | 111.7 |
| Dihedral angle (°) | | |
| N1—C19—C1—C6 | 71.09 | 82.59 |

### 3.4. DFT calculations

Theoretical calculations using DFT method at B3LYP/6-311++G(d,p) level of theory have been performed in order to get insights into the electronic properties, chemical reactivity, and molecular structure of the synthesized compounds. Compound **4b**, of which we have its experimental coordinates, was chosen as a representative molecule. Firstly, a full geometry optimization has been carried out, and the most stable structure has been compared with the experimental results obtained by single-crystal structure analysis. The atom-by-atom superimposition of the optimized molecular structure of compound **4b** on the crystal structure, and selected calculated and experimental geometry parameters are shown in Fig. 5 and Table 4, respectively. As can be seen, the theoretical and experimental structures are perfectly aligned. The bond lengths and angles of the two structures have nearly the same values. The only difference was observed for the dihedral angle of the phenyl ring, which is slightly deviated by about 10°.

After successfully optimized the molecular structure of compound **4b**, we then calculated, at the same level of theory, some electronic and structural properties such as frontier molecular orbitals (FMO), molecular electrostatic potential mapping, atomic charge distributions, and physicochemical descriptors.

The study of the energy and distribution of frontier molecular orbitals provides valuable insights into chemical stability and reactivity as well as potential biological mechanisms of organic compounds [45,47,48,50,66–68]. In terms of chemical reactivity, the

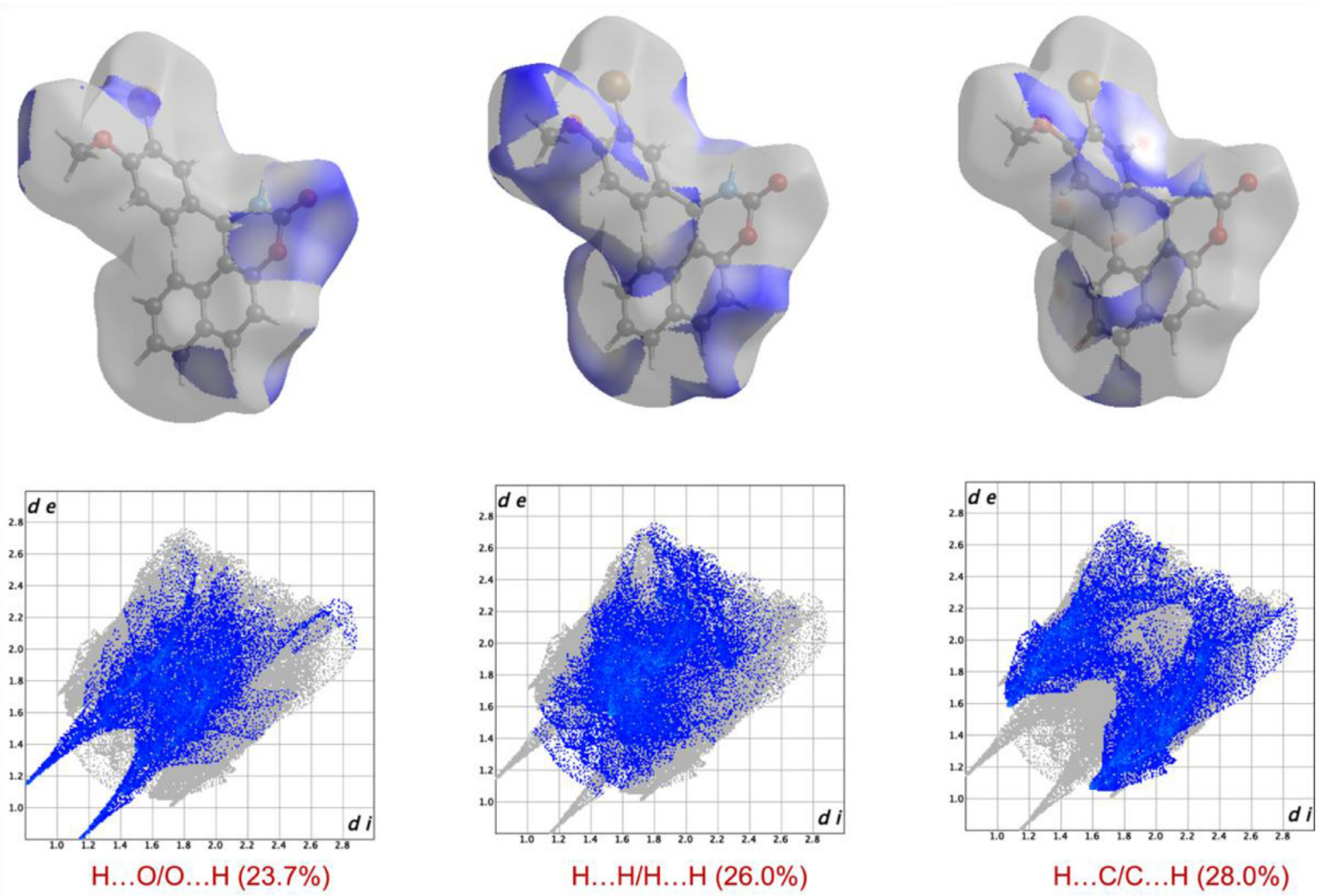


**Fig. 4.** The 2D fingerprints of compound **4b** resolved into, H…O/O…H, H…H/H…H, and H…C/C…H contacts (blue areas).

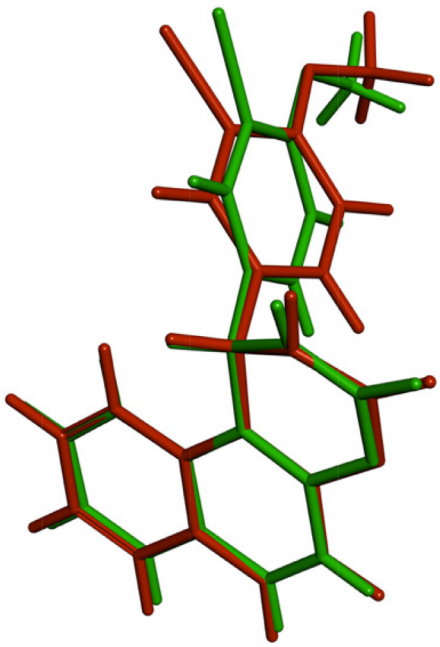

**Fig. 5.** Atom-by-atom superimposition of the optimized molecular structure of compound **4b** (red) on the crystal structure (green).

distribution of FMO could be used to determine the sites of electrophilic and nucleophilic attacks. HOMO (highest occupied molecular orbital) is the easiest orbital to donate electrons and determines the sites for nucleophilic attacks, while LUMO (lowest unoccupied molecular orbital) is the easiest orbital to accept electrons and determines the sites for electrophilic attacks. The energy gap of HOMO-LUMO could be used to estimate the chemical stability and reactivity of molecules. The calculated HOMO-LUMO energies and distributions of compound **4b** are depicted in Fig 6. The obtained results show that both the HOMO and LUMO are mainly distributed on the naphtyle moiety with small distributions on the phenyl and oxazinone rings. This indicates that the electronic charges are mainly located on the naphtyle moiety. The values of HOMO (-6.39 eV) and LUMO (-1.78 eV) and their energy gap (4.61 eV) indicate a high kinetic stability and low chemical reactivity of compound **4b** [69,70].

It is well established that several physicochemical properties such as vibrational spectroscopy, stability, chemical reactivity, electrostatic potential, dipole moment, and solubility are mainly determined by the distribution of electrons within molecules [71,72]. The atomic charge distribution of compound **4b** has been calculated using the Mulliken atomic charges method. The obtained results are presented in Table S4 in SI and visualized in Fig. 7. As shown, the highest negative charges were found to be localized around the oxygen atom of the carbony group, and the nitrogen atom with partial charges of -0.305 and -0.225 respectively. While, the highest positive charges were found for carbons 14, 18, and

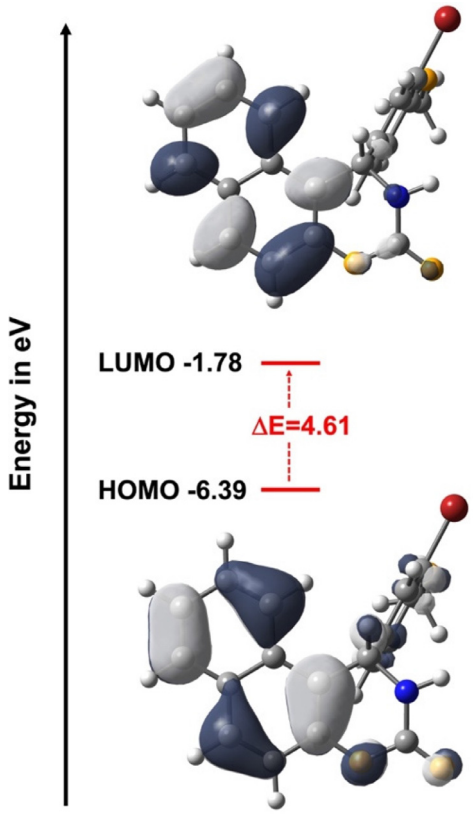


**Fig. 6.** HOMO and LUMO of compound **4b** computed at B3LYP/6-311++G(d,p) level of theory in the gas-phase.

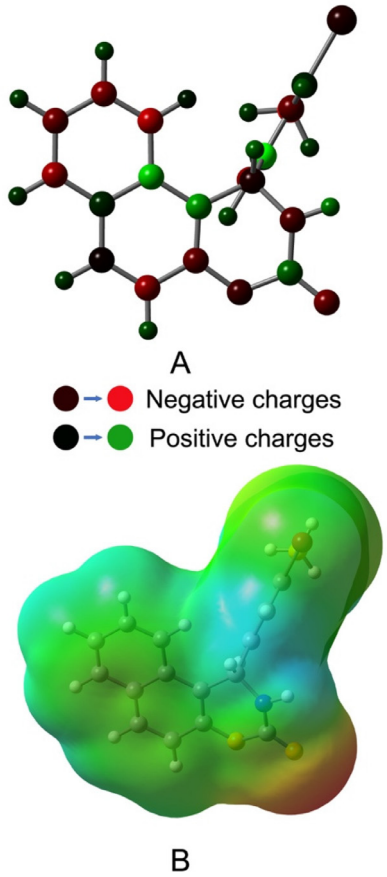


**Fig. 7.** Mulliken atomic charges (A) and molecular electrostatic potential (B) of compound **4b** computed at B3LYP/6-311++G(d,p) level of theory in the gas-phase.

17 and the hydrogen atom of the NH bond with partial charges of 0.848, 0.569, 0.427, and 0.335 respectively.

Molecular electrostatic potential (ESP) was also computed to visualize the electronic charge distribution of compound **4b**. Fig. 7 shows the obtained 3D mapped molecular electrostatic potential. As can be seen, the obtained results are in good agreement with Mulliken atomic charges distribution. The highest negative charges are mainly localized around the oxygen atom of the carbonyl group, suggesting that this atom should be the most privileged site for nucleophilic attack. Whereas, the highest positive regions are around the hydrogen of the NH bond and the carbon C14, indicating that these regions should be the most favorable sites for electrophilic attacks.

Physicochemical indicators such as electronegativity ($\chi$), chemical hardness ($\eta$), chemical softness (S), and electrophilic index ($\omega$) are important quantitative properties that characterizes the chemical stability and reactivity of organic compounds [73–75]. $\chi$ indicates the capacity of a molecule to attract electrons. $\eta$ and S are indications of resistance to charge transfer. $\omega$ is defined as a measure of energy lowering associated with a maximum amount of electron flow between a donor and an acceptor [73–75]. All the mentioned physicochemical indicators were calculated for compound **4b** using the frontier molecular orbitals method. The obtained results are shown in Table S5 in SI. It was found that compound **4b** presents a chemical hardness value of 2.31 eV and a chemical softness value of 0.22 eV, suggesting a good kinetic stability and low chemical reactivity. In terms of electronegativity and electrophilic index, compound **4b** is characterized by relatively high values when compared to some typical antioxidants [47]. This indicates that the electron acceptance capacity of compound **4b** is better than its electron donation capacity.

### 3.5. Biology evaluation

#### 3.5.1. Evaluation of AChE and BChE inhibition

The inhibitory potencies of selected compounds **4b-4f** toward AChE and BChE were evaluated using Ellman's assay [53] as described previously in detail. The inhibition studies were carried out and experimental results were reported in Table 5. Galantamine was used as a control for its ability to inhibit both ChEs. The results of AChE inhibition revealed that all selected compounds showed good to moderate degree of inhibition with $IC_{50}$ values ranging from 9.30 to 137.33 µM. The 4-phenyl-$C_6H_4$ derivative **4c** with $IC_{50}$ value of 9.30±0.10 µM was found to be the most potent compound against AChE. This compound was 2.3 times more potent than the standard drug galantamine. It should be noted that compounds **4b** and **4f** showed $IC_{50}$ values in the same range. The least active compounds were found to be **4e** and **4d**, with $IC_{50}$ values equal to 125.16 and 137.33 $\mu$M, respectively.

Analyzing the structure-activity relationship (SAR), we could observe that the nature of substituents on the aromatic ring plays a significant role on the inhibitory potency of AChE. The best result was obtained with the biphenyl derivative **4c** substituent at para position. Also, as observed with compounds **4b** and **4f** (bromine-substituted), the 2-bromo or 3-bromo-4-methoxy substituents on phenyl ring improved anti-AChE activity. In contrast, the insertion of thiophenyl or ethyl group at the ortho or para position resulted in a noticeable decrease in the inhibitory activity.

In terms of inhibitory activity against BChE, all the tested compounds showed mild to moderate activities with $IC_{50}$ values in the range of 2.30–240.45 µM. The best result was obtained with compound **4b**, which shows an $IC_{50}$ value (2.30±0.04 $\mu$M)

**Table 5**
Cholinesterase and $\alpha$-Glucosidase inhibitory activities of selected compounds.

| Compound | AChE$IC_{50}$ ± SD (μM)[a] | BChE$IC_{50}$ ± SD (μM)[a] | Selectivity[b] | $\alpha$-Glucosidase$IC_{50}$ ± SD (μM)[a] |
|---|---|---|---|---|
| 4b | 21.24 ± 0.01 | 2.30 ± 0.04 | 0.11 | 49.63 ± 1.81 |
| 4c | 9.30 ± 0.10 | 18.56 ± 0.60 | 1.99 | 41.07 ± 0.76 |
| 4d | 137.33 ± 0.72 | 75.03 ± 0.24 | 0.55 | 95.27 ± 0.89 |
| 4e | 125.16 ± 0.65 | 240.45 ± 2.21 | 1.92 | 77.63 ± 0,52 |
| 4f | 16.56 ± 0.37 | 178.97 ± 4,38 | 10.81 | 42.53 ± 1,01 |
| Galantamine[c] | 21.82 ± 4.00 | 40.72 ± 2.85 | 1.87 | Nt |
| Ascarbose[c] | Nt | Nt | - | 426.62 ± 2.46 |
| Quercetin[c] | Nt | Nt | - | 12.35 ± 0.38 |

[a] Values expressed are means ± S.D. of three parallel measurements.
[b] Selectivity ratio: $IC_{50}$ (BChE)/ $IC_{50}$ (AChE)
[c] Reference compounds. Nt: Not tested.

17.7 times lower than that of the reference drug galantamine ($IC_{50}$ = 40.72 ± 2.85 $\mu$M). From the SAR point of view, there was almost similarity between BChE and AChE. All the tested compounds **4b-4f** acted as selective AChE inhibitors, with selectivity index ranging from 0.11 to 10.81.

### 3.5.2. Evaluation of $\alpha$-glucosidase inhibitory activity

The *in vitro* $\alpha$-glucosidase inhibitory activity of the synthesized compounds **4b-4f** were carried out according to the protocol of S. Lordan et *al* with minor modification [54], using quercetin and acarbose as reference compounds for comparative purposes. The obtained results are presented in Table 5. It was found that all the tested compounds are inhibitors of $\alpha$-glucosidase with a varying efficiency, having $IC_{50}$ values ranging from 41.07±0.76 to 95.27±0.89 $\mu$M. Compound **4c** having biphenyl group was found to be the most active compound in the series. The second most active compound is **4f** (42.53 ± 1,01 $\mu$M) having a bromo at the position 2 of phenyl ring. Similarly, inhibitory activity of compounds **4b, 4e**, and **4d** was significantly higher than that of acarbose ($IC_{50}$ = 426.62 ± 2.46 $\mu$M), with $IC_{50}$ value of 49.63, 77.63 and 95.27 $\mu$M, respectively. By comparison, all of the tested compounds were found to be more potent than acarbose and less potent than quercitin.

### 3.6. Molecular docking studies

Docking studies have been performed for the most active compounds (**4b** and **4c**) in order to rationalize the permission experimental results. The interactions of both the *R* and *S* enantiomers of compound **4b** with the active site of AChE (PDB ID: 4EY6), as well as the two isomers of compound **4c** at the active site of BChE (PDB ID: 4BDS) and $\alpha$-glucosidase (PDB: 5ZCB) have been investigated. For comparative purposes, the docking study has been also performed for the standards galantamine and quercetin. The obtained results of the most energetically favorable binding modes of these compounds at the active sites of the studied enzymes are shown in Table 6. As seen from the table, the obtained binding energies are in good agreement with the *in vitro* studies. The interactions of all the studied compounds with the target receptors are characterized by low binding energies ranging from −8.0 kcal/mol to −13.1 kcal/mol, comparable or lower than those of the studied standards.

The binding mode of the *R* and *S* enantiomers of compound **4b** and **4c** at the active site of AChE, BChE, and $\alpha$-glucosidase are depicted in Figs. 8–10. As shown in Fig. 8, both the enantiomers of compound **4c** interact with the active site of AChE by forming several $\pi$-$\pi$ stacking between TRP86, TYR 124, and TYR337 residues and the phenyl and naphtyl moieties of compound **4c**. The *(R)* enantiomer form also a strong intermolecular hydrogen bond with the residue GLY122. These residues are involved in ligand-receptor interaction of several commercialized

**Table 6**
Binding energies in kcal/mol of the (*R*)- and (*S*)-enantiomers of the most active compounds (**4b** and **4c**) and the standards galantamine and quercetin with AChE (PDB ID: 4EY6), BChE (PDB ID: 4BDS), and $\alpha$-glucosidase (PDB: 5ZCB).

| Compound | Binding energies (kcal/mol) | | |
|---|---|---|---|
| | AChE | BChE | $\alpha$-Glucosidase |
| (*R*)-4b | Nd | −9.0 | Nd |
| (*S*)-4b | Nd | −9.6 | Nd |
| (*R*)-4c | −11.7 | Nd | −8.0 |
| (*S*)-4c | −13.1 | Nd | −8.2 |
| Galantamine | −10.1 | −9.2 | Nd |
| Quercetin | Nd | Nd | −8.2 |

Nd: not determined

AChE inhibitors such as Galantamaine, Huperzine A, Tacrine, and Donepezil [56].

The best poses of the interactions of the *R* and *S* enantiomers of compound **4b** with BChE enzyme are presented in Fig. 9. As can be seen, both the enantiomers of compound **4b** interact by intermolecular hydrogen bonds, $\pi$-$\pi$ stacking, and hydrophobic interacts with residues GLY117, HIS438, and ALA328. The *R* enantiomer of compound **4b** forms also a hydrogen bond with the residue TRP82. The residues GLY117, HIS438, and TRP82 are located in the oxyanion hole, catalytic triad, and anionic site of the active site of BChE respectively, which could explain the low $IC_{50}$ value of compound **4b** [76,77].

As for the $\alpha$-glucosidase enzyme, the enantiomers of compound **4b** do not interact with the same amino acid residues (Fig. 10). The *R* enantiomer is expected to form three hydrogen bonds with GLU408 and LYS334 as well as two hydrophobic interactions with ASN333 and LUS373. While, the *S* enantiomer forms two hydrogen bonds with HIS108 and TYR68, one carbon hydrogen bond with ASP67, and several hydrophobic interactions with LYS69 and GLU180.

As can be concluded from the above discussion, the expected interactions, together with the predicted binding affinity for the potent molecules (**4b** and **4c**) suggest that these compounds should show significant AChE, BChE, and $\alpha$-glucosidase inhibitory activities, which is in good agreement with the *in vitro* studies.

### 3.7. In silico *ADME analysis*

In drug development, good pharmacological activity is not enough for a compound to become a drug candidate because so many compounds fail in clinical trials due to poor pharmacokinetic properties. There are four main components of pharmacokinetics: absorption, distribution, metabolism and excretion (ADME). These are used to explain the varied characteristics of different drugs in the body. In order to evaluate the pharmacokinetic properties of the synthesized compounds **4a-4f**, the ADME parameters of all the compounds have been calculated using Molinspiration software

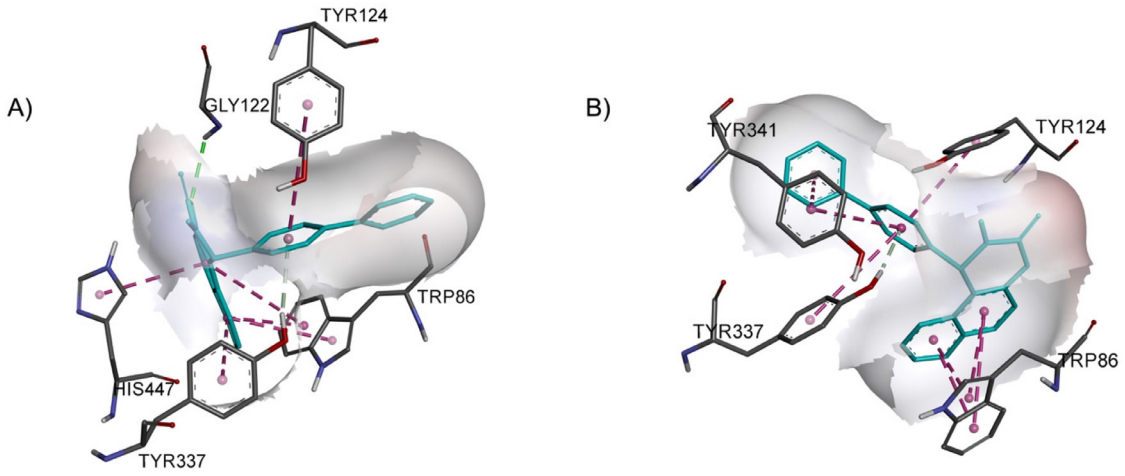


**Fig. 8.** Docking poses of compounds **(*R*)-4c** (A) and **(*S*)-4c** (B) in the active site of AChE enzyme.

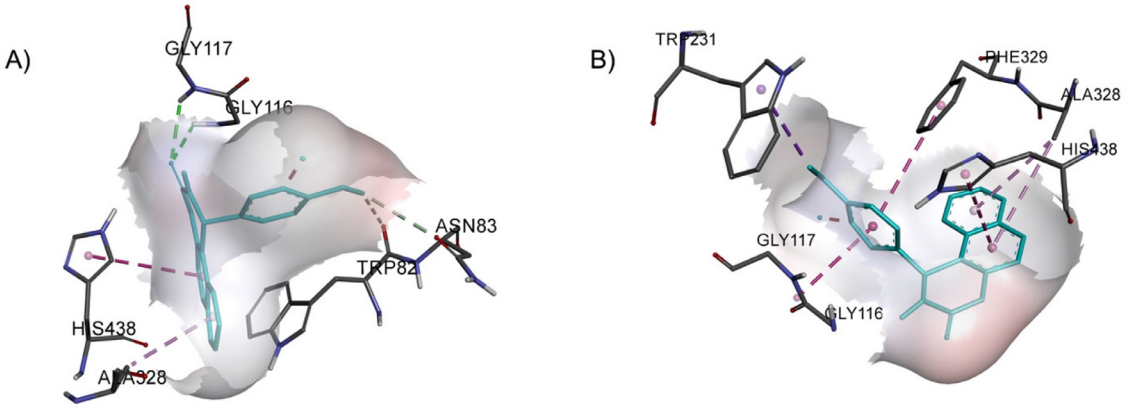


**Fig. 9.** Docking poses of compounds **(*R*)-4b** (A) and **(*S*)-4b** (B) in the active site of BChE enzyme.

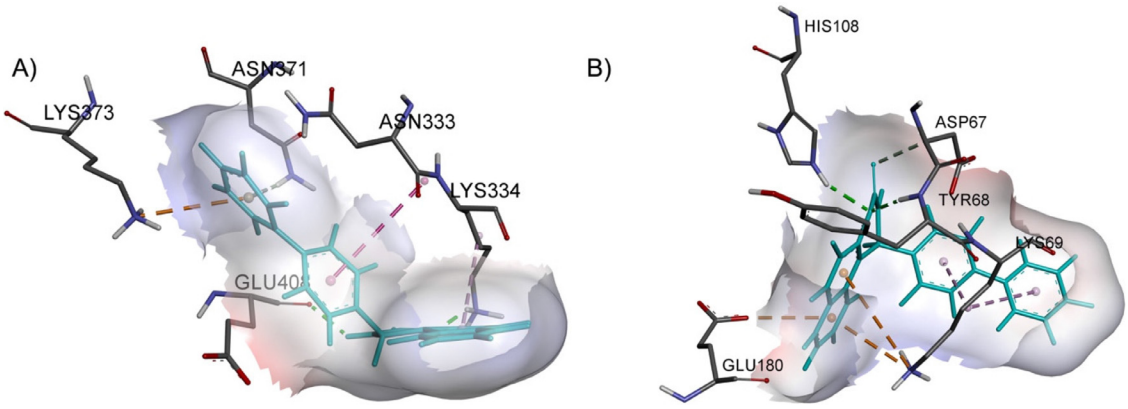


**Fig. 10.** Docking poses of compounds **(*R*)-4c** (A) and **(*S*)-4c** (B) in the active site of $\alpha$-glucosidase enzyme.

and the obtained results are tabulated in Table S7 in SI. According to the Lipinski's rule [78], each potential drug should have no more than one violation of the following criteria: (1) molecular mass less than or equal to 500 daltons (optimum around 300 daltons); (2) number of hydrogen bond acceptors less than or equal to 10 (optimum of approximately 5); (3) number of hydrogen bond donors less than or equal to 5 (optimum of 2); and (4) lipophilic character measured by the logarithm of the partition coefficient P, ie log P greater than or equal to -2 and less than or equal to 5 (optimum around 3). An examination of the obtained results reported in Table S7 indicates that all the studied compounds perfectly respect the Lipinski's rule (no more than one violation of the mentioned criteria). In addition, all the compounds were shown an excellent percentage of absorption ranging from 92.58 % to 95.77 %, which indicates that they are easily absorbed by the human body [79]. These results suggest that compounds **4a-4f** have excellent pharmacokinetic properties and could be considered as promising drug candidates.

## 4. Conclusion

In this work we have reported an environmentally friendly synthesis of a series of naphthoxazine derivatives (**4a-4f**) using phenylboronic acid as catalyst. Molecular structures of the synthesized compounds were confirmed by FTIR, NMR and HRMS methods and, for compound **4b,** by single crystal X-ray diffraction analysis. The AChE, BChE, and $\alpha$-glucosidase inhibitory activities of compounds **4b-4f** were investigated *in vitro*. The obtained results revealed that all of the studied compounds exhibit good to moderate degree of inhibition against the investigated enzymes. Compound **4c** was found to be the best AChE inhibitor with an $IC_{50}$ value lower than that of galantamine. While, compound **4b** presented the best BChE and $\alpha$-glucosidase inhibitory activities with $IC_{50}$ values lower than those of galantamine and acarbose. On the other hand, the molecular structure, chemical reactivity, stability, and biological activity of the synthesized compounds were investigated by theoretical calculations and molecular modeling. The obtained results revealed great correlation between experimental and theoretical studies. Based on our findings, the synthesized naphthoxazine derivatives provide promising starting points for further research to develop new drugs for the treatment of AD and DM.

## Declaration of Competing Interest

The authors declare that they have no known competing financial interests or personal relationships that could have appeared to influence the work reported in this paper.

## CRediT authorship contribution statement

**Khawla Boudebbous:** Investigation. **Houssem Boulebd:** Software, Formal analysis, Writing - original draft, Visualization, Writing - review & editing. **Chamseddine Derabli:** Writing - original draft. **Lamia Bendjeddou:** Investigation. **Chawki Bensouici:** Resources. **Dominique Harakat:** Resources. **Hocine Merazig:** Resources. **Abdelmadjid Debache:** Conceptualization, Supervision.

## Acknowledgments

We would like to thank MESRS (Ministère de l'Enseignement Supérieur et de la Recherche Scientifique, Algeria) and DGRSDT (Direction Générale de la Recherche Scientifique et du développement Technologique, Algeria) for financial support.

## Supplementary materials

Supplementary material associated with this article can be found, in the online version, at doi:10.1016/j.molstruc.2020.129103.

## References

[1] L.W. Mohamed, S.M. Abuel-Maaty, W.A. Mohammed, M.A. Galal, Synthesis and biological evaluation of new oxopyrrolidine derivatives as inhibitors of acetyl cholinesterase and $\beta$ amyloid protein as anti–Alzheimer's agents, Bioorg. Chem. 76 (2018) 210–217.
[2] K.Y. Yeong, W.-L. Liew, V. Murugaiyah, C.W. Ang, H. Osman, S.C. Tan, Ethyl nitrobenzoate: A novel scaffold for cholinesterase inhibition, Bioorg. Chem. 70 (2017) 27–33.
[3] D.J. Selkoe, M.B. Podlisny, Deciphering the genetic basis of Alzheimer's disease, Annu. Rev. Genomics Hum. Genet. 3 (1) (2002) 67–99.
[4] F. Zemek, L. Drtinova, E. Nepovimova, V. Sepsova, J. Korabecny, J. Klimes, K. Kuca, Outcomes of Alzheimer's disease therapy with acetylcholinesterase inhibitors and memantine, Expert Opin. Drug Saf. 13 (6) (2014) 759–774.
[5] D. Muñoz-Torrero, Acetylcholinesterase inhibitors as disease-modifying therapies for Alzheimer's disease, Curr. Med. Chem. 15 (24) (2008) 2433–2455.
[6] L. Scotti, F. Jaime Bezerra Mendonça Junior, M. Sobral da Silva, I.R. Pitta, M. Tullius Scotti, Biochemical changes evidenced in Alzheimer's disease: a mini-review, Lett. Drug Des. Discovery 11 (2) (2014) 240–248.
[7] R.P. Sequeira, Central nervous system stimulants, drugs that suppress appetite, and drugs used in Alzheimer's disease, Side Eff. Drugs Annu. 25 (2002) 1–12 Elsevier.
[8] S.P. Kasturi, S. Surarapu, S. Uppalanchi, S. Dwivedi, P. Yogeeswari, D.K. Sigalapalli, N.B. Bathini, K.S. Ethiraj, J.S. Anireddy, Synthesis, molecular modeling and evaluation of $\alpha$-glucosidase inhibition activity of 3, 4-dihydroxy piperidines, Eur. J. Med. Chem. 150 (2018) 39–52.
[9] S.R. Joshi, E. Standl, N. Tong, P. Shah, S. Kalra, R. Rathod, Therapeutic potential of $\alpha$-glucosidase inhibitors in type 2 diabetes mellitus: an evidence-based review, Expert Opin. Pharmacother. 16 (13) (2015) 1959–1981.
[10] M.J. Mphahlele, N.M. Magwaza, S. Gildenhuys, I.B. Setshedi, Synthesis, $\alpha$-glucosidase inhibition and antioxidant activity of the 7-carbo–substituted 5-bromo-3-methylindazoles, Bioorg. Chem. (2020) 103702.
[11] N.H.A. Alkefai, S. Amin, M. Sharma, J. Ahamad, S.R. Mir, New olean-15-ene type gymnemic acids from Gymnema sylvestre (Retz.) R. Br. and their antihyperglycemic activity through $\alpha$-glucosidase inhibition, Phytochem. Lett. 32 (2019) 83–89.
[12] L. Kumar, K. Lal, P. Yadav, A. Kumar, A.K. Paul, Synthesis, characterization, $\alpha$-glucosidase inhibiton and molecular modeling studies of some pyrazoline-1H-1, 2, 3-triazole hybrids, J. Mol. Struct. (2020) 128253.
[13] J.D. Howe, N. Smith, M.-R. Lee, N. Ardes-Guisot, B. Vauzeilles, J. Désiré, A. Baron, Y. Blériot, M. Sollogoub, D.S. Alonzi, Novel imino sugar $\alpha$-glucosidase inhibitors as antiviral compounds, Bioorg. Med. Chem. 21 (16) (2013) 4831–4838.
[14] K.J. Dougherty, B.A. Bannatyne, E. Jankowska, P. Krutki, D.J. Maxwell, Membrane receptors involved in modulation of responses of spinal dorsal horn interneurons evoked by feline group II muscle afferents, J. Neurosci. 25 (3) (2005) 584–593.
[15] M. Anderluh, J. Cesar, P. Štefanič, D. Kikelj, D. Janeš, J. Murn, K. Nadrah, M. Tominc, E. Addicks, A. Giannis, Design and synthesis of novel platelet fibrinogen receptor antagonists with 2H-1, 4-benzoxazine-3 (4H)-one scaffold. A systematic study, Eur. J. Med. Chem. 40 (1) (2005) 25–49.
[16] R.S. Bethiel, J. Cochran, Y.-C. Moon, S. Nanthakumar, Inhibitors of c-Jun N-terminal kinases (JNK) and other protein kinases, Google Patents (2005).
[17] M. Patel, S.S. Ko, R.J. McHugh Jr, J.A. Markwalder, A.S. Srivastava, B.C. Cordova, R.M. Klabe, S. Erickson-Viitanen, G.L. Trainor, S.P. Seitz, Synthesis and evaluation of analogs of Efavirenz (SUSTIVATM) as HIV-1 reverse transcriptase inhibitors, Bioorg. Med. Chem. Lett. 9 (19) (1999) 2805–2810.
[18] O.M.O. Habib, H.M. Hassan, A. El-Mekabaty, Studies on some benzoxazine-4-one derivatives with potential biological activity, Am. J. Org. Chem. 2 (3) (2012) 45–51.
[19] P.Y. Johnson, R. Silver, The synthesis and antitumor properties of a 6-Alkoxy tetrahydrooxazine, J. Heterocycl. Chem. 10 (6) (1973) 1029–1030.
[20] G.Y. Lesher, A.R. Surrey, A new method for the preparation of 3-substituted-2-oxazolidones, J. Am. Chem. Soc. 77 (3) (1955) 636–641.
[21] H.S. Mosher, M.B. Frankel, M. Gregory, Heterocyclic diphenylmethane derivatives, J. Am. Chem. Soc. 75 (21) (1953) 5326–5328.
[22] H. Ren, S. Grady, D. Gamenara, H. Heinzen, P. Moyna, S.L. Croft, H. Kendrick, V. Yardley, G. Moyna, Design, synthesis, and biological evaluation of a series of simple and novel potential antimalarial compounds, Bioorg. Med. Chem. Lett. 11 (14) (2001) 1851–1854.
[23] F. Benedini, G. Bertolini, R. Cereda, G. Dona, G. Gromo, S. Levi, J. Mizrahi, A. Sala, New antianginal nitro esters with reduced hypotensive activity. Synthesis and pharmacological evaluation of 3-[(nitrooxy) alkyl]-2H-1, 3-benzoxazin-4 (3H)-ones, J. Med. Chem. 38 (1) (1995) 130–136.
[24] S. Knapp, Synthesis of complex nucleoside antibiotics, Chem. Rev. 95 (6) (1995) 1859–1876.
[25] E. Juaristi, V.A. Soloshonok, Enantioselective Synthesis of Beta-Amino Acids, John Wiley & Sons, 2005.
[26] R. Mannhold, H. Kubinyi, Molecular Biology in Medicinal Chemistry, John Wiley & Sons, 2006.
[27] M. Dabiri, A.S. Delbari, A. Bazgir, A novel three-component, one-pot synthesis of 1, 2-dihydro-1-arylnaphtho [1, 2-e][1, 3] oxazine-3-one derivatives under microwave-assisted and thermal solvent-free conditions, Synlett (05) (2007) 0821–0823 2007.
[28] M. Dabiri, A. Sadat Delbari, A. Bazgir, A simple and environmenttally benign method for the synthesis of naphthoxazin-3-one derivatives, Heterocycles 71 (3) (2007) 543–548.
[29] N. Montazeri, E.M. Nezhad, Tetramethylammonium hydroxide (TMAH) as an efficient catalyst for the one-pot synthesis of 1, 2-dihydro-1-aryl-naphtho [1, 2-e][1, 3] oxazine-3-ones under solvent-free conditions, Bull. Chem. Soc. Ethiop. 30 (1) (2016) 161–164.
[30] K. Nikna, P. Abolpour, Synthesis of naphthoxazinone derivatives using silica-bonded S-sulfonic acid as catalyst under solvent-free conditions, J. Chem. Sci. 127 (7) (2015) 1315–1320.
[31] M. Lei, L. Ma, L. Hu, Highly chemoselective condensation of $\beta$-naphthol, aldehyde, and urea catalyzed by thiamine hydrochloride, Synth. Commun. 41 (22) (2011) 3424–3432.
[32] R. Hunnur, R. Kamble, A. Dorababu, B.S. Kumar, C. Bathula, TiCl4: An efficient catalyst for one-pot synthesis of 1, 2-dihydro-1-aryl-naphtho-[1, 2-e][1, 3] oxazin-3-one derivatives and their drug score analysis, Arabian J. Chem. 10 (2017) S1760–S1764.
[33] A. Kumar, A. Saxena, M. Dewan, A. De, S. Mozumdar, Recyclable nanoparticulate copper mediated synthesis of naphthoxazinones in PEG-400: a green approach, Tetrahedron Lett. 52 (38) (2011) 4835–4839.

[34] G.B.D. Rao, M.P. Kaushik, A.K. Halve, An efficient synthesis of naphtha [1, 2-e] oxazinone and 14-substituted-14H-dibenzo [a, j] xanthene derivatives promoted by zinc oxide nanoparticle under thermal and solvent-free conditions, Tetrahedron Lett. 53 (22) (2012) 2741–2744.

[35] K. Boudebbous, H. Boulebd, C. Bensouici, D. Harakat, R. Boulcina, A. Debache, Synthesis, docking study and biological activities evaluation of 1-amidoalkyl-2-naphthol derivatives as dual inhibitors of cholinesterase and $\alpha$-glucosidase, ChemistrySelect 5 (19) (2020) 5515–5520.

[36] C. Derabli, I. Boualia, A.B. Abdelwahab, R. Boulcina, C. Bensouici, G. Kirsch, A. Debache, A cascade synthesis, in vitro cholinesterases inhibitory activity and docking studies of novel Tacrine-pyranopyrazole derivatives, Bioorg. Med. Chem. Lett. 28 (14) (2018) 2481–2484.

[37] I. Boualia, C. Derabli, R. Boulcina, C. Bensouici, M. Yildirim, A. Birinci Yildirim, E.H. Mokrani, A. Debache, Synthesis, molecular docking studies, and biological evaluation of novel alkyl bis (4-amino-5-cyanopyrimidine) derivatives, Archiv der Pharmazie 352 (11) (2019) 1900027.

[38] H. Boulebd, L. Ismaili, H. Martin, A. Bonet, M. Chioua, J. Marco Contelles, A. Belfaitah, New (benz) imidazolopyridino tacrines as nonhepatotoxic, cholinesterase inhibitors for Alzheimer disease, Fut. Med. Chem. 9 (8) (2017) 723–729.

[39] A. Altomare, G. Cascarano, C. Giacovazzo, A. Guagliardi, Completion and refinement of crystal structures with SIR92, J. Appl. Crystallogr. 26 (3) (1993) 343–350.

[40] G.M. Sheldrick, SHELXT–Integrated space-group and crystal-structure determination, Acta Crystallogr. Sect. A 71 (1) (2015) 3–8.

[41] L.J. Farrugia, WinGX and ORTEP for Windows: an update, J. Appl. Crystallogr. 45 (4) (2012) 849–854.

[42] C.F. Macrae, P.R. Edgington, P. McCabe, E. Pidcock, G.P. Shields, R. Taylor, M. Towler, J.V.D. Streek, Mercury: visualization and analysis of crystal structures, J. Appl. Crystallogr. 39 (3) (2006) 453–457.

[43] A.D. Becke, Density-functional exchange-energy approximation with correct asymptotic behavior, Phys. Rev. A 38 (6) (1988) 3098.

[44] P.C. Hariharan, J.A. Pople, The influence of polarization functions on molecular orbital hydrogenation energies, Theor. Chim. Acta 28 (3) (1973) 213–222.

[45] H. Boulebd, Y.D. Lahneche, I.A. Khodja, M. Benslimane, A. Belfaitah, New Schiff bases derived from benzimidazole as efficient mercury-complexing agents in aqueous medium, J. Mol. Struct. 1196 (2019) 58–65.

[46] J. Tirado-Rives, W.L. Jorgensen, Performance of B3LYP density functional methods for a large set of organic molecules, J. Chem. Theory Comput. 4 (2) (2008) 297–306.

[47] H. Boulebd, Comparative study of the radical scavenging behavior of ascorbic acid, BHT, BHA and Trolox: Experimental and theoretical study, J. Mol. Struct. 1201 (2020) 127210.

[48] H. Boulebd, DFT study of the antiradical properties of some aromatic compounds derived from antioxidant essential oils: C–H bond vs. O–H bond, Free Radic. Res. 53 (11-12) (2019) 1125–1134.

[49] H. Boulebd, I. Amine Khodja, M.V. Bay, N.T. Hoa, A. Mechler, Q.V. Vo, Thermodynamic and kinetic studies of the radical scavenging behavior of hydralazine and dihydralazine: theoretical insights, J. Phys. Chem. B 124 (20) (2020) 4123–4131.

[50] H. Boulebd, The role of benzylic-allylic hydrogen atoms on the antiradical activity of prenylated natural chalcones: a thermodynamic and kinetic study, J. Biomol. Struct. Dyn. (2020) 1–10.

[51] M.J. Frisch, G.W. Trucks, H.B. Schlegel, G.E. Scuseria, M.A. Robb, J.R. Cheeseman, G. Scalmani, V. Barone, B. Mennucci, G.A. Petersson, H. Nakatsuji, M. Caricato, X. Li, A.F.I.H.P. Hratchian, J. Bloino, G. Zheng, M.H.J.L. Sonnenberg, M. Ehara, K. Toyota, J.H.R. Fukuda, M. Ishida, T. Nakajima, Y. Honda, H.N.O. Kitao, T. Vreven, J.A. Montgomery Jr, F.O.J.E. Peralta, M.J. Bearpark, J. Heyd, K.N.K.E.N. Brothers, V.N. Staroverov, R. Kobayashi, K.R.J. Normand, A.P. Rendell, J.C. Burant, J.T.S.S. Iyengar, M. Cossi, N. Rega, N.J. Millam, J.E.K.M. Klene, J.B. Cross, V. Bakken, C. Adamo, R.G.J. Jaramillo, R.E. Stratmann, O. Yazyev, R.C.A.J. Austin, C. Pomelli, J.W. Ochterski, K.M.R.L. Martin, V.G. Zakrzewski, G.A. Voth, J.J.D.P. Salvador, S. Dapprich, A.D. Daniels, J.B.F. ¨O. Farkas, J.V. Ortiz, J. Cioslowski, D.J. Fox, Gaussian 09, Gaussian, Inc., Wallingford CT, 2009.

[52] M.J. Turner, J.J. McKinnon, S.K. Wolff, D.J. Grimwood, P.R. Spackman, D. Jayatilaka, M.A. Spackman, CrystalExplorer (Version 17.5), (2017).

[53] G.L. Ellman, K.D. Courtney, V. Andres, R.M. Featherstone, A new and rapid colorimetric determination of acetylcholinesterase activity, Biochem. Pharmacol. 7 (2) (1961) 88–95.

[54] S. Lordan, T.J. Smyth, A. Soler-Vila, C. Stanton, R.P. Ross, The $\alpha$-amylase and $\alpha$-glucosidase inhibitory effects of Irish seaweed extracts, Food Chem. 141 (3) (2013) 2170–2176.

[55] I. Sánchez-Linares, J.M. H. Pérez-Sánchez, J.M. Cecilia, García, High-throughput parallel blind virtual screening using BINDSURF, BMC Bioinformatics 13 (14) (2012) S13.

[56] J. Cheung, M.J. Rudolph, F. Burshteyn, M.S. Cassidy, E.N. Gary, J. Love, M.C. Franklin, J.J. Height, Structures of human acetylcholinesterase in complex with pharmacologically important ligands, J. Med. Chem. 55 (22) (2012) 10282–10286.

[57] F. Nachon, E. Carletti, C. Ronco, M. Trovaslet, Y. Nicolet, L. Jean, P.-Y. Renard, Crystal structures of human cholinesterases in complex with huprine W and tacrine: elements of specificity for anti-Alzheimer's drugs targeting acetyl- and butyryl-cholinesterase, Biochem. J. 453 (3) (2013) 393–399.

[58] W. Auiewiriyanukul, W. Saburi, K. Kato, M. Yao, H. Mori, Function and structure of GH13_31 $\alpha$-glucosidase with high $\alpha$-(1→4)-glucosidic linkage specificity and transglucosylation activity, FEBS Lett. 592 (13) (2018) 2268–2281.

[59] S.S. Kottawar, S.A. Siddiqui, S.R. Bhusare, A novel one-pot synthesis of 1, 2-dihydro-1-phenyl-naphtho [1, 2-e][1, 3] oxazin-3-ones, Rasayan J. Chem. 3 (2010) 646–648.

[60] H.A. Ahangar, G.H. Mahdavinia, K. Marjani, A. Hafezian, A one-pot synthesis of 1, 2-dihydro-1-arylnaphtho [1, 2-e][1, 3] oxazine-3-one derivatives catalyzed by perchloric acid supported on silica (HClO 4/SiO 2) in the absence of solvent, J. Iran. Chem. Soc. 7 (3) (2010) 770–774.

[61] M. Sharma, S. Manohar, D.S. Rawat, Lewis acid catalyzed synthesis of 1-Aryl208;1, 2-dihydro-naphtho [1, 2-e][1, 3] oxazin-3-ones under solvent free conditions: a mechanistic approach, J. Heterocycl. Chem. 49 (3) (2012) 589–595.

[62] F.H. Allen, O. Kennard, D.G. Watson, L. Brammer, A.G. Orpen, R. Taylor, Tables of bond lengths determined by X-ray and neutron diffraction. Part 1. Bond lengths in organic compounds, J. Chem. Soc., Perkin Trans. 2 (12) (1987) S1–S19.

[63] A. Bazgir, V. Amani, H.R. Khavasi, Methyl N-[(2-hydroxynaphthalen-1-yl)(phenyl) methyl] carbamate, Acta Crystallogr. Sect. E 62 (8) (2006) o3533–o3534.

[64] D.T. Cremer, J.A. Pople, General definition of ring puckering coordinates, J. Am. Chem. Soc. 97 (6) (1975) 1354–1358.

[65] M.C. Etter, Encoding and decoding hydrogen-bond patterns of organic compounds, Acc. Chem. Res. 23 (4) (1990) 120–126.

[66] A. Nataraj, V. Balachandran, T. Karthick, Molecular structure, vibrational spectra, first hyperpolarizability and HOMO–LUMO analysis of p-acetylbenzonitrile using quantum chemical calculation, J. Mol. Struct. 1038 (2013) 134–144.

[67] B.W. Clare, Frontier orbital energies in quantitative structure-activity relationships: a comparison of quantum chemical methods, Theor. Chim. Acta 87 (6) (1994) 415–430.

[68] I. Amine Khodja, C. Bensouici, H. Boulebd, Combined experimental and theoretical studies of the structure-antiradical activity relationship of heterocyclic hydrazone compounds, J. Mol. Struct. 1221 (2020) 128858.

[69] Y.-Y. Cai, L.-Y. Xu, L.-Q. Chai, Y.-X. Li, Synthesis, crystal structure, TD/DFT calculations and Hirshfeld surface analysis of 1-(4-((Benzo)dioxol-5-ylmethyleneamino)phenyl)ethanone oxime, J. Mol. Struct. 1204 (2020) 127552.

[70] M. Kumar, M. Kariem, H.N. Sheikh, A. Frontera, S.K. Seth, A.K. Jassal, A series of 3D lanthanide coordination polymers decorated with a rigid 3,5-pyridinedicarboxylic acid linker: syntheses, structural diversity, DFT study, Hirshfeld surface analysis, luminescence and magnetic properties, Dalton Trans. 47 (35) (2018) 12318–12336.

[71] İ. Sıdır, Y.G. Sıdır, M. Kumalar, E. Taşal, Ab initio Hartree–Fock and density functional theory investigations on the conformational stability, molecular structure and vibrational spectra of 7-acetoxy-6-(2,3-dibromopropyl)-4,8-dimethylcoumarin molecule, J. Mol. Struct. 964 (1) (2010) 134–151.

[72] K. Padmavathy, K.G. Krishnan, C.U. Kumar, P. Sutha, R. Sivaramakarthikeyan, C. Ramalingan, Synthesis, antioxidant evaluation, density functional theory study of dihydropyrimidine festooned phenothiazines, ChemistrySelect 3 (21) (2018) 5965–5974.

[73] P.K. Chattaraj, U. Sarkar, D.R. Roy, Electrophilicity Index, Chem. Rev. 106 (6) (2006) 2065–2091.

[74] R.G. Parr, L.V. Szentpály, S. Liu, Electrophilicity Index, J. Am. Chem. Soc. 121 (9) (1999) 1922–1924.

[75] R. Praveena, K. Sadasivam, V. Deepha, R. Sivakumar, Antioxidant potential of orientin: a combined experimental and DFT approach, J. Mol. Struct. 1061 (2014) 114–123.

[76] F. Nachon, L. Ehret-Sabatier, D. Loew, C. Colas, A. van Dorsselaer, M. Goeldner, Trp82 and Tyr332 are involved in two quaternary ammonium binding domains of human butyrylcholinesterase as revealed by photoaffinity labeling with [3H]DDF, Biochemistry 37 (29) (1998) 10507–10513.

[77] P. Masson, P. Legrand, C.F. Bartels, M.-T. Froment, L.M. Schopfer, O. Lockridge, Role of Aspartate 70 and Tryptophan 82 in binding of succinyldithiocholine to human butyrylcholinesterase, Biochemistry 36 (8) (1997) 2266–2277.

[78] C.A. Lipinski, F. Lombardo, B.W. Dominy, P.J. Feeney, Experimental and computational approaches to estimate solubility and permeability in drug discovery and development settings, Adv. Drug. Deliv. Rev. 23 (1-3) (1997) 3–25.

[79] Y.H. Zhao, M.H. Abraham, J. Le, A. Hersey, C.N. Luscombe, G. Beck, B. Sherborne, I. Cooper, Rate-limited steps of human oral absorption and QSAR studies, Pharm. Res. 19 (10) (2002) 1446–1457.